Self-Organizing Fuzzy Rule-Based Approach for Muons Classification in High Energy Physics

Ualison R. F. Dias * **Luciano M. A. Filho** * **José M. de Seixas** ** **Eduardo P. de Aguiar** *

* *Federal University of Juiz de Fora, MG, (e-mail: {ualison.dias,luciano.andrade,eduardo.aguiar}@engenharia.ufjf.br)*
** *Federal University of Rio de Janeiro, RJ, (e-mail: seixas@lps.ufrj.br)*

Abstract: In Particle Physics, the aim is to probe deeper into understanding the structure of matter. For this, collider experiments are essential tools to prove theories experimentally and discover whether there is new physics beyond the Standard Model of Particle Physics. In this regard, muons are important signatures for many interesting physics processes. Thus, this work presents an enhanced approach based on Self-Organizing Fuzzy Classifiers applied to the muon classification. Experimental results are included and discussed, showing the effectiveness of Self-Organizing Fuzzy Classifiers in the solution of the problem at hand.

Keywords: Muon classification; self-organizing fuzzy classifiers; particle accelerators; fuzzy system; computational intelligence.

1. INTRODUCTION

Several researchers aim to discover how our universe was created and its nature. These are complex questions and are difficult to answer. Nowadays, the Standard Model summarizes the best of our knowledge (Gaillard et al., 1999). This model describes three of the four known fundamental forces, which are electromagnetic, weak, strong interactions. However, the gravitational force is not well described within the Standard Model (Gell-Mann, 2018). Scientists worldwide developed this model during the latter half of the twentieth century. Even though the model is currently the better description, it does not explain everything. There is more behind this to prove the theories made experimentally and to discover beyond the Standard Model.

Since then, several machines aiming at particle acceleration have been built based on the principle of electromagnetic fields to provide particles with very high energy and speed. As a result, there are over 30,000 accelerators worldwide with a diversified focus, for example, physics research.

Focusing on searches physics, the accelerators, as the name same implies, are used to accelerate the particles close to the speed of light. It is not only one particle, but particles beam in opposite directions through-beam pipes kept at an ultrahigh vacuum.When the high energy collision happens into these pipes, phenomena such as the production of other elementary particles occur. Since the significant goals are understanding and studying the produce generated, we can analyze the gradual decay of particles. Thus, identifying and measuring properties and quantities of the physical events and finding the particles mass, speed, and charge.

Intending to study the subproducts of collisions, the high-energy experiments are placed around the collision point and comprise different detectors (Adriani et al., 2008). The tracking detectors measure the trajectories of charged particles (Granja et al., 2021); calorimeters measure the energies of incoming particles (Wigmans, 2017) and the muon spectrometer (Policicchio, 2019). At LHC, ATLAS is the largest experiment (Iengo et al., 2010). ATLAS is a general-purpose experiment, as it was designed to cover all the important physics channels that are being studied in the LHC (Schmidt, 2016).

In ATLAS, Tilecal (Di Girolamo, 2000) is the main hadronic calorimeter. Tilecal is segmented into layers of cells and produces almost ten thousand signals, which are produced from scintillating fibers and readout from photomultiplier tubes (PMTs) (Xia et al., 2015). The signals are conditioned, amplified, and digitized, so their amplitudes are proportional to the energy deposited in each cell. Figure 1 displays a typical Tilecal signal.

The last Tilecal layer is sufficiently large to produce coincidence information with the muon spectrometer and, thus, may be used to improve muon detection (Adragna et al., 2009). Actually, Tilecal has been assisting the online muon filter through an FPGA-based digitizing board (TMDB - Tile-Muon Digitizer Board) (Henriques, 2015). Presently, a matched-filter approach is applied for detecting muons from the collision vertex, which allows the discarding of fake muons and improves the data acquisition bandwidth (Takeda, 2019). Alternative models to improve muon detection have been proposed using machine learning (Liu et al., 2019) and, more specifically, deep learning techniques (Nguyen et al., 2019). These more complex models might still be embedded in modern FPGAs for online applications.

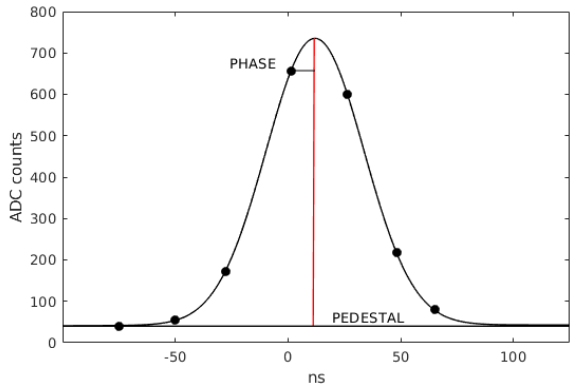

Figure 1. Pulse shape of an typical analog signal.

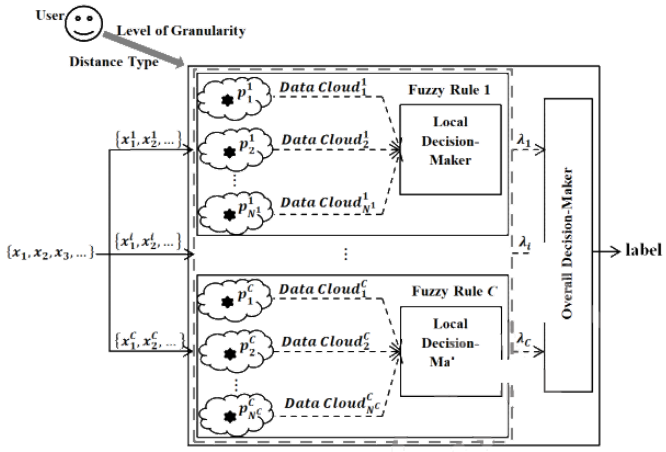

Figure 2. Architecture of the Self-Organizing Fuzzy Logic (SOF) classifier (Gu and Angelov, 2018).

This paper conducts a preliminary study for an improved variation of the Self-Organizing Fuzzy Logic Classifier (SOF) for muon detection and envisages such an embedded application in ATLAS. The design project was proposed in Gu and Angelov (2018), and we added several distance metrics to Dias et al. (2019). The SOF method is non-parametric because its meta-parameters are derived from the data. However, it allows users to decide the level of granularity and the type of distance/dissimilarity. The model provides even more freedom for the user, making the approach adaptable to different applications. Mahalanobis and Euclidean distances and cosine dissimilarity are used in the original model, and we adopted three other distance metrics, Hamming, Minkowski, and Manhattan, to get higher accuracy.

2. A NEW APPROACH FOR MUON DETECTION

2.1 Self-Organizing Fuzzy Logic Classifier

SOFs are nonparametric classifiers that can identify prototypes from the data set observed and use in online and offline training. In the first stage, offline training employed these prototypes to build an inference system based on rules of type *AnYa* of order 0 (Angelov and Yager, 2012) then it is applied for classification. In the original model, Gu and Angelov (2018) the authors used how distance metrics: Mahalanobis, Euclidean, and Cosine. In this paper, we propose additional distance metrics, such as Hamming, Minkowski, and Manhattan. We have done it in order to gain muon detection accuracy.

In the second stage, we have the offline mode, where SOF can learn continuously from the data stream following any data pattern change, and their structure updates the total time. We can see the architecture of the model in Figure 2.

As mentioned earlier, the prototypes are defined and used to determine the rules based on the model in the offline stage. We summarize this stage in the algorithm below:

Algorithm 1 Offline training process of the SOF
[1] Calculate D^{MM} at $\{\mathbf{u}\}^c_{U^c_K}$; Find $\mathbf{r}_1 = \arg max(\mathrm{D}^{MM}_{K^c}(\mathbf{u}^c_i))$ and exclude $\mathbf{r}_1$ from $\{\mathbf{u}\}^c_{U^c_K}$; $k \leftarrow 1$; $\{\mathbf{r}\} \leftarrow \mathbf{r}_1$; $\{D^{MM}_{K^c}(\mathbf{r})\} \leftarrow D^{MM}_{K^c}(\mathbf{r}_1)$;;
$U^c_K \neq 0$
* $k \leftarrow k+1$;
* Find $\mathbf{r}_k = \arg min(d(\mathbf{r}_{k-1}, \mathbf{u}^c_i)$ and exclude $\mathbf{r}_k$ from $\{\mathbf{u}\}^c_{U^c_K}$;
* $\{\mathbf{r}\} \leftarrow \{\mathbf{r}\} + \mathbf{r}_k$; $\{D^{MM}_{K^c}(\mathbf{r})\} \leftarrow \{D^{MM}_{K^c}(\mathbf{r})\} + D^{MM}_{K^c}(\mathbf{r}_k)$;
Identify $\{\mathbf{p}_0\}$; Organize data clouds around $\{\mathbf{p}\}_0$; Identify $\{\varphi\}_0$ from of data clouds; Calculate D^{MM} em $\{\varphi\}_0$; Identify $\{\varphi\}^{neighboring}$; Identify $\{\mathbf{p}\}^c$; Make a c^{th} fuzzy rule with $\{\mathbf{p}\}^c$;

where $\{\mathbf{u}\}^c_{U^c_K}$ is the data set used, without samples repeat. D^{MM} is a multimodal density, $\mathbf{r}$ is a list where the samples are classified under their respective multimodal density. $\mathbf{p}_0$ represent the prototypes of the data, $\{\varphi\}_0$ are the data clouds centers neighboring the cloud i, and $\{\mathbf{p}\}^c$ is o prototype more significant of the c^{th} class.

In the online stage, the rules identified are updated from streaming data, following the potential changes in these data. This stage is summarized at Algorithm 2, where $\mu^c_{k^c}$, $X^c_{k^c}$ and $\Sigma^c_{k^c}$ are meta-parameter of the model. $\mathbf{G}^{c,L}_{k^c}$ is the average radius of local areas of influence, N^c is the support (number of members) of c^{th} data clouds.

SOF is a nonparametric model that derives a meta-parameter from the data set. We can decide the level of granularity and what possibility to do a trade-off between performance and computational efficiency.

The approach allows the user to choose distance metrics employed in the algorithm's calculation. This choice gives even more freedom to the user, making the method highly adaptable to a large variety of applications.

Algorithm 2 Online training process of the SOF classifier [1] a new data sample of c^{th} class $x^c_{k^c+1}$ is available Update $\mu^c_{k^c}$, $X^c_{k^c}$, $\Sigma^c_{k^c}$, $\mathbf{G}^{c,L}_{k^c}$ to $\mu^c_{k^c+1}$, $X^c_{k^c+1}$, $\Sigma^c_{k^c+1}$, $\mathbf{G}^{c,L}_{k^c+1}$; Calculate D at $x^c_{k^c+1}$ e $\{\mathbf{p}\}^c$; a new prototype is added to the rule) *or* (a new prototype and a new cloud is added to the rule)
* $N^c \leftarrow \mathrm{N}^c + 1$; $\mathbf{p}^c_{N^c} \leftarrow \mathrm{x}^c_{k^c+1}$; $\mathbf{S}^c_{N^c} \leftarrow 1$;$\{\mathrm{p}\}^c \leftarrow \{\mathrm{p}\}^c + \mathbf{p}^c_{N^c}$;
* Find $\mathbf{p}^c_{n^*}$;
* $\mathbf{p}^c_{n^*} \leftarrow \frac{\mathbf{S}^c_{n^*}}{\mathbf{S}^c_{n^*}+1}\mathrm{p}^c_{n^*} + \frac{1}{\mathbf{S}^c_{n^*}+1}x^c_{k^c+1}$; $\mathbf{S}^c_{n^*} \leftarrow \mathrm{S}^c_{n^*} + 1$; $K^c \leftarrow \mathrm{K}^c + 1$; Update the fuzzy rule;

For further information regarding the calculation of the variables involved in the two stages of the approach, see Gu and Angelov (2018). The algorithm used in this paper are available at `https://github.com/ualisondias/SOFtoMuonDetection`.

2.2 Distance metrics

In the paper Gu and Angelov (2018) the authors suggest the utilization of the Mahalanobis, Euclidean, and Cosine distances. We will use three more distances to gain accuracy in the muon's classification.

Considering that the data set is $\mathbf{R}^N$, defined as $\{\mathbf{x}\}_K = \{\mathbf{x}_1, \mathbf{x}_2, ..., \mathbf{x}_K\} \in \mathbf{R}^N; \mathbf{x}_i = [x_{i,1}, x_{i,2}, ..., x_{i,N}]^T; i, j = 1, 2, ..., K$, where the indices denote individual samples. $\mathbf{x}_K$ can be presented in the matrix form:

$$\mathbf{X}_K = [\mathbf{x}_1, \mathbf{x}_2, ..., \mathbf{x}_K] = \begin{bmatrix} x_{1,1} & x_{2,1} & ... & x_{K,1} \\ x_{1,2} & x_{2,2} & ... & x_{K,2} \\ \vdots & \vdots & \vdots & \vdots \\ x_{1,N} & x_{2,N} & ... & x_{K,N} \end{bmatrix} \tag{1}$$

These distance metrics between $\mathbf{x}_i$; $\mathbf{x}_j$ and $\{\mathbf{x}\}_K$ adopted in this paper are defined in Angelov and Gu (2019).

Euclidean distance Euclidean distance is commonly used, their efficiency and validity as the distance metric, in the majority of cases, are granted. The calculation of the distance between two points is given as:

$$d_{euc}(x_i, x_j) = ||\mathbf{x}_i - \mathbf{x}_j|| = \sqrt{\sum_{l=1}^{N}(x_{i,l} - x_{j,l})^2} \tag{2}$$

Mahalanobis distance Considering that the model follows a Gaussian distribution or some similar, we can choose Mahalanobis distance. It is a distance that uses a covariance between the points given as:

$$d_{mah}(x_i, x_j) = \sqrt{(x_i - x_j)^T C_K^{-1}(x_i - x_j)} \tag{3}$$

where $\mu_k = \frac{1}{K}\sum_{i=1}^{K}\mathbf{x}_i$; C_K is the covariance matrix of $\{\mathbf{x}\}_K$ given as:

$$C_K = \frac{1}{K}\sum_{i=1}^{K}(x_i - \mu_K)(x_i - \mu_K)^T \tag{4}$$

Cosine distance Approaches whose dimensions are large, cosine distance can be practical.

$$d_{cos}(x_i, x_j) = \cos(\theta_x^{i,j}) \tag{5}$$

where $\theta_x^{i,j}$ represent the angle between x_i and x_j. Then we can represent the inner product of two vectors as:

$$d_{cos}(\mathbf{x}_i, \mathbf{x}_j) = \frac{\langle \mathbf{x}_i, \mathbf{x}_j \rangle}{\|\mathbf{x}_i\| \, \|\mathbf{x}_j\|} \tag{6}$$

where $\langle \mathbf{x}_i, \mathbf{x}_j \rangle = \sum_{l=1}^{N} x_{i,l}x_{j,l}$ and $\|\mathbf{x}_i\| = \sqrt{\langle \mathbf{x}_i, \mathbf{x}_j \rangle}$.

Hamming distance We used the hamming distance to represent semantic complex structures with high fidelity. It is the percentage of coordinate that is different, given as:

$$d_{ham}(x_i, x_j) = \frac{(x_i \neq x_j)}{N} \tag{7}$$

where N is the number of samples.

Minkowski distance We use the Minkowski distance when it is necessary to identify and, in fact, ignore irrelevant characteristics and when there are many anomalous conglomerates. The metric is a normed vector space that can generalize the Euclidean distance, the Manhattan distance, and Chebyshev distance, it is given by:

$$d_{min}(\mathbf{x}_i, \mathbf{x}_j) = \left(\sum_{l=1}^{N}(|x_{i,l} - x_{j,l}|)^p\right)^{\frac{1}{p}} \tag{8}$$

where $0 \leq p \leq 2$.

Manhattan distance We use the Manhattan distance where the relative importance of characteristics must be considered, being that it is a pondered version between two normed vectors. This metrics are included in the same family of distance functions, where it is a special case of Minkowski for $p = 1$:

$$d_{man}(x, y) = \sum_{l=1}^{N}(|x_{i,l} - x_{j,l}|) \tag{9}$$

In this preliminary study, several metrics were tested to determine whether they are more susceptible to adapting to the problems identified.

3. EXPERIMENTAL RESULTS

In this section, we will briefly summarize our data set. We have used a toy Monte Carlo simulation, similar to the one presented in Luciano Filho et al. (2015). This simulation has focused on signal generation, provided for the synthetic generation of different calorimeter pulse shapes and signal-to-noise ratios. Regarding this, we have a flexible simulation; in contrast, we also have a limited scope.

In the simulation of a calorimeter, several assembly characteristics have to be considered, like the collider luminosity,

the calorimeter type (electromagnetic or hadronic), the sensor layer and pseudorapidity. Some of these characteristics and the relationship with muon will be more explained.

Several steel plates are put around the electromagnet calorimeter. As we know the muon's decay process, we can verify only our region of interest η, where it represents a spatial coordinate named pseudorapidity. It is commonly used by experimental physics to describe the angle of a particle relative to the beam axis, and we represent it as:

$$\eta = \frac{1}{2}\ln(tan\frac{\theta}{2}) \tag{10}$$

In Figure 3 we can see an illustration of pseudorapidity.

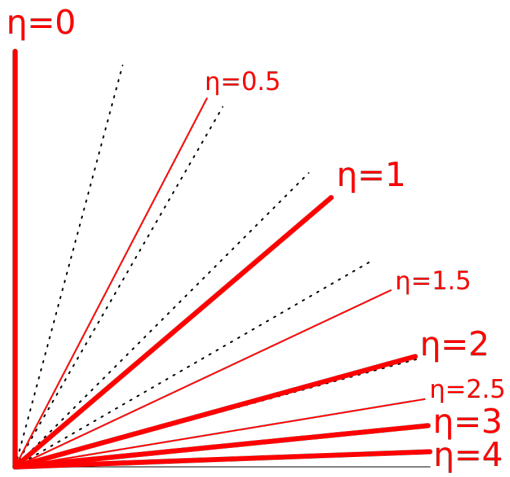

Figure 3. Pseudorapidity values shown on a polar plot.

Therefore, if we have known that a particle crosses our interest region and with a determined momentum transverse (***pt***), it may be a muon candidate. The momentum transverse can be determined as:

$$p_x = p_T \cos\phi \tag{11}$$
$$p_y = p_T \sin\phi \tag{12}$$
$$p_z = p_T \sinh\eta \tag{13}$$

Consequently, we have:

$$p_T = \sqrt{p_x^2 + p_y^2}\,|p| = \cosh\eta \tag{14}$$

Therefore, with these expressions, we can find the transversal moment and the pseudorapidity, which are essential for constructing a muon detector. The system that we use in this paper is the segmented calorimeter, counting on several cells and resulting in thousands of channels. One part is divided into some modules, and each module is further segmented into layers of readout cells with a specified value of granularity.

When occurring, the interaction between particles and steel creates shower stalls of more moderate energy particles, which produce light when passing through the scintillating tiles. Fibers transmit the light to a photomultiplier

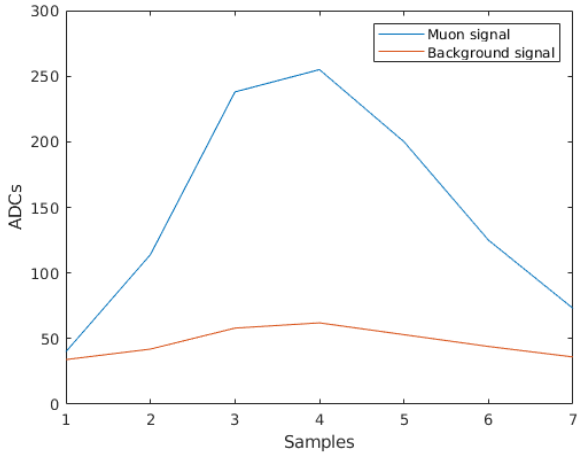

Figure 4. Pulse shape of muon and background signals.

(PMTs) and then convert this light into electrical signals. After this conversion, all signals are processed by a card that handles signal conditioning and amplification beyond processing. The signals are then digitized by 10-bit Analog-to-Digital Converts (ADCs) in the digitizer boards.

In this mode, we have a data set composted by many signals labeled as background and muon signals after being validated. In Figure 4, we can see two accurate signals. In blue, we have a muon signal, and an orange, we have a background signal.

When dealing with many signals, be them muon or background, our fundamental challenge is to identify and classify what it is, as the shape of the pulse is not always well defined. As in our data set, we have 10,000 background signals, and several signals can easily be mistakenly identified as a muon signals.

In Figure 5, we can see the whole plot signals of the background with three marked signals that have a shape similar to a muon signal, and already in Figure 6, we have a zoom in the signal with this aspect.

Thus, when we compare the shape of the muon signal and the background signal, they are very similar. In Figure 7, you can see this in two signs. Therefore, it is not easy to classify these signals in this case.

The simulations were carried out with 20,000 samples. Which 10,000 for background and 10,000 for the muon. It is randomly divided into 10,000 for the testing phase, 8,000 for the offline training phase, and 2,000 for the online training phase. It was necessary to normalize this data set between 0 and 1. The algorithm used in this paper are available in `https://github.com/ualisondias/SOFforMuonDetection`.

We are using Accuracy Score, F-Score, Kappa and RMSE to evaluate the model. Accuracy is commonly used to measure the observational error, which is how close or far a given set of measurements is to their true value. F-Score, also known as balanced F-score, can be interpreted as a harmonic mean of precision and recall. The relative contribution of precision and recall to the F1 score are equal. Furthermore, Cohen's kappa is a statistic that measures and expresses the level of agreement between two

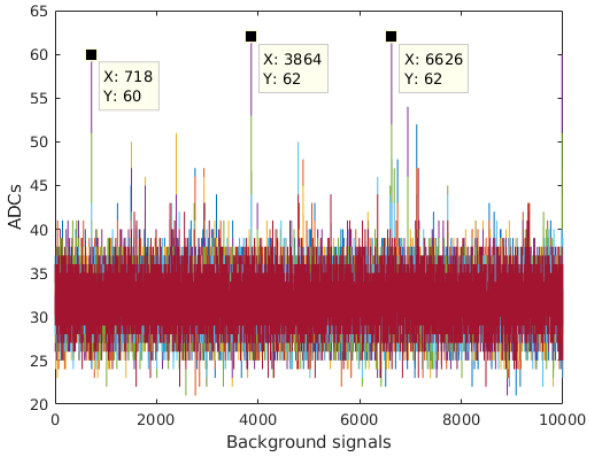

Figure 5. Background signals.

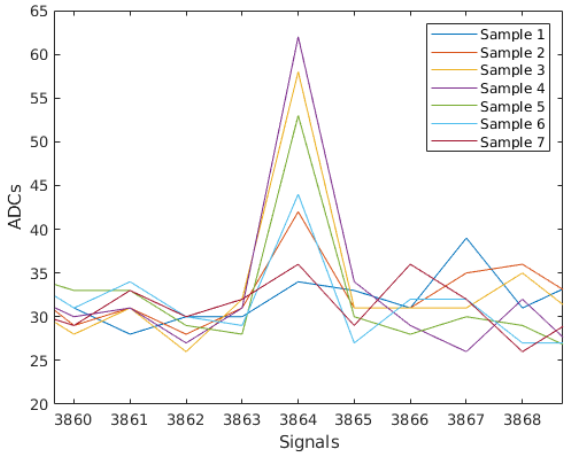

Figure 6. Zoom in of signal 3864.

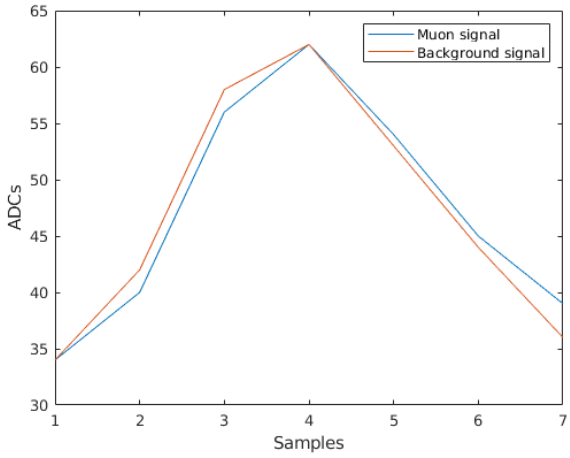

Figure 7. Comparison muon and background signals.

annotators on a classification problem. In addition, we also have the RMSE metric, that root-mean-square error, a risk metric corresponding to the expected value of the squared error or loss.

Table 1. Preliminary results of the training process.

	Accuracy	F-Score	Kappa	RMSE
Cosine	1	1	1	0
Euclidean	1	1	1	0
Mahalanobis	0,9995	0,9995	0,999	0,02236
Minkowski	1	1	1	0
Hamming	1	1	1	0
Manhattan	1	1	1	0

Table 2. Preliminary results of the testing process.

	Accuracy	F-Score	Kappa	RMSE
Cosine	0,8108	0,8114	0,6216	0,4350
Euclidean	0,8412	0,8406	0,6824	0,3985
Mahalanobis	0,6264	0,7187	0,2528	0,6112
Minkowski	0,8398	0,8404	0,6799	0,4002
Hamming	0,7707	0,7691	0,5414	0,4788
Manhattan	0,8363	0,8372	0,6726	0,4046

The preliminary results of this paper are in Table 1, and you can see for the training process, except for Mahalanobis distance, all the others got a 100% score of accuracy, F-Score, and Kappa, and as expected the low value of RMSE. The preliminary results of this paper are in Table 2, and you can see for the testing process, except for Mahalanobis distance, all the others obtained a 100% score of accuracy, F-Score, Kappa, and as expected, the low value of RMSE.

We obtained preliminary results for the test process, which can be seen in Table 2. The best precision results were for the Euclidean and Minkowski distances, which were close. The other models had satisfactory results, around 80 %. In all cases, except for the Mahalanobis distance, this approach offers high Kappa and F-score values and low MSE values. The results gathered in the tables show that the proposals are attractive for the muon classification problem.

The better results for Euclidean can be explained by the fact that this distance is more generalist and has the shortest distance between two points, as the data have no outliers. Moreover, Euclidean distance is commonly used for Gaussian problems, similar to the present case. In the same way, we have a good result on Minkowski distance, and it is because the distance is a metric in a normed vector space which can be considered as a generalization of the Euclidean distance.

4. CONCLUSION

This work presents an enhanced approach based on the self-organizing fuzzy classifiers applied to muon classification using a toy Monte Carlo simulation that generates a data set composed of muon and background signal samples. The fuzzy classifier proved to be independent of pre-defined parameters or previous assumptions, as it is driven only by empirically observed data. The SOF identifies prototypes of the training data and continues to learn through the data with the data flow recursively. As a way to compare the model, several distance metrics were used. Experimental results showed that the proposed model presented high accuracy, F-score, Kappa coefficient,

and lower mean square error when applied to a data set composed of muon and background signals.

As a sign for future works, we intend to apply the enhanced SOF in the online processing of streaming data related to muon classification using an FPGA device. Besides, we will present the model discussed in this work and join other models aiming the better results for muon classification to help professionals in the decision-making processes and devise strategies in the research.

ACKNOWLEDGMENTS

The authors would like to thank CNPq, CAPES, FAPERJ and FAPEMIG for their support to this work.

REFERENCES

Adragna, P., Alexa, C., Anderson, K., Antonaki, A., Arabidze, A., Batkova, L., Batusov, V., Beck, H., Bednar, P., Kuutmann, E.B., et al. (2009). Testbeam studies of production modules of the atlas tile calorimeter. *Nuclear Instruments and Methods in Physics Research Section A: Accelerators, Spectrometers, Detectors and Associated Equipment*, 606(3), 362–394.

Adriani, O., Bonechi, L., Bongi, M., Castellini, G., D'Alessandro, R., Faus, D., Fukui, K., Grandi, M., Haguenauer, M., Itow, Y., et al. (2008). The lhcf detector at the cern large hadron collider. *Journal of Instrumentation*, 3(08), S08006.

Angelov, P. and Yager, R. (2012). A new type of simplified fuzzy rule-based system. *International Journal of General Systems*, 41(2), 163–185.

Angelov, P.P. and Gu, X. (2019). *Empirical approach to machine learning*. Springer.

Di Girolamo, B. (2000). The atlas tilecal hadronic calorimeter. *Nuclear Instruments and Methods in Physics Research Section A: Accelerators, Spectrometers, Detectors and Associated Equipment*, 453(1-2), 233–236.

Dias, U., Aguiar, E., Hell, M., Medeiros, A., and Silveira, D. (2019). Self-organizing fuzzy rule-based approach for dealing with the classification of indoor environments for iot applications. In *Proceedings of 16th National Meeting on Artificial and Computational Intelligence*, 1044–1055. SBC.

Gaillard, M.K., Grannis, P.D., and Sciulli, F.J. (1999). The standard model of particle physics. *Reviews of Modern Physics*, 71(2), S96.

Gell-Mann, M. (2018). The eightfold way: A theory of strong interaction symmetry. In *The Eightfold Way*, 11–57. CRC Press.

Granja, C., Oancea, C., Jakubek, J., Marek, L., Benton, E., Kodaira, S., Miller, J., Rucinski, A., Gajewski, J., Stasica, P., et al. (2021). Wide-range tracking and let-spectra of energetic light and heavy charged particles. *Nuclear Instruments and Methods in Physics Research Section A: Accelerators, Spectrometers, Detectors and Associated Equipment*, 988, 164901.

Gu, X. and Angelov, P.P. (2018). Self-organising fuzzy logic classifier. *Information Sciences*, 447, 36–51.

Henriques, A. (2015). The atlas tile calorimeter. In *2015 4th International Conference on Advancements in Nuclear Instrumentation Measurement Methods and their Applications (ANIMMA)*, 1–7. IEEE.

Iengo, P., Collaboration, A., et al. (2010). Status and performace of the atlas experiment. *Nuclear Physics B-Proceedings Supplements*, 207, 91–94.

Liu, B., Xiong, X., Hou, G., Song, S., and Shen, L. (2019). Applications of machine learning at besiii. In *EPJ Web of Conferences*, volume 214, 06033. EDP Sciences.

Luciano Filho, M.d.A., Peralva, B.S., de Seixas, J.M., and Cerqueira, A.S. (2015). Calorimeter response deconvolution for energy estimation in high-luminosity conditions. *IEEE Transactions on Nuclear Science*, 62(6), 3265–3273.

Nguyen, T.Q., Weitekamp, D., Anderson, D., Castello, R., Cerri, O., Pierini, M., Spiropulu, M., and Vlimant, J.R. (2019). Topology classification with deep learning to improve real-time event selection at the lhc. *Computing and Software for Big Science*, 3(1), 1–14.

Policicchio, A. (2019). The phase-ii upgrade of the atlas muon spectrometer. Technical report, ATL-COM-MUON-2019-050.

Schmidt, B. (2016). The high-luminosity upgrade of the lhc: Physics and technology challenges for the accelerator and the experiments. In *Journal of Physics: Conference Series*, volume 706, 022002. IOP Publishing.

Takeda, K. (2019). Software-based data acquisition system for level-1 end-cap muon trigger in atlas run-3. In *EPJ Web of Conferences*, volume 214, 01036. EDP Sciences.

Wigmans, R. (2017). *Calorimetry: Energy Measurement in Particle Physics*, volume 168. Oxford University Press.

Xia, J., Qian, S., Wang, W., Ning, Z., Cheng, Y., Wang, Z., Li, X., Qi, M., Heng, Y., Liu, S., et al. (2015). A performance evaluation system for photomultiplier tubes. *Journal of Instrumentation*, 10(03), P03023.